

S4-Net: Geometry-Consistent Semi-Supervised Semantic Segmentation

Sinisa Stekovic¹

Friedrich Fraundorfer¹

Vincent Lepetit^{1,2}

¹Institute for Computer Graphics and Vision, Graz University of Technology, Graz, Austria

²Laboratoire Bordelais de Recherche en Informatique, University of Bordeaux, Bordeaux, France

{sinisa.stekovic, fraundorfer, lepetit}@icg.tugraz.at

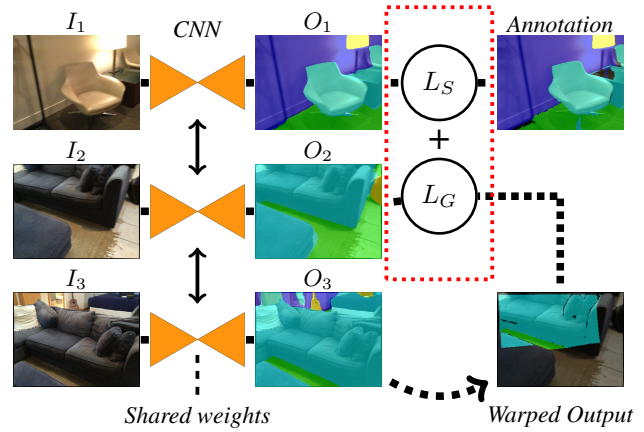
Abstract

We show that it is possible to learn semantic segmentation from very limited amounts of manual annotations, by enforcing geometric 3D constraints between multiple views. More exactly, image locations corresponding to the same physical 3D point should all have the same label. We show that introducing such constraints during learning is very effective, even when no manual label is available for a 3D point, and can be done simply by employing techniques from 'general' semi-supervised learning to the context of semantic segmentation. To demonstrate this idea, we use RGB-D image sequences of rigid scenes, for a 4-class segmentation problem derived from the ScanNet dataset. Starting from RGB-D sequences with a few annotated frames, we show that we can incorporate RGB-D sequences without any manual annotations to improve the performance, which makes our approach very convenient. Furthermore, we demonstrate our approach for semantic segmentation of objects on the LabelFusion dataset, where we show that one manually labeled image in a scene is sufficient for high performance on the whole scene.

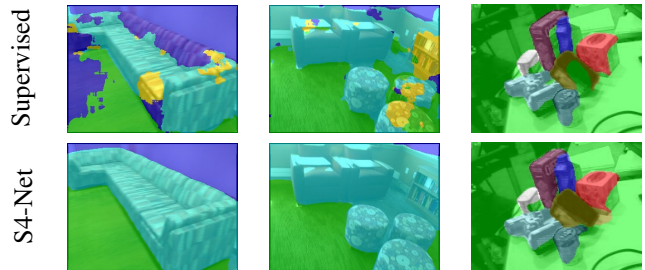
1. Introduction

Semantic segmentation of images provides high-level understanding of a scene, which is useful in many applications including robotics and augmented reality. Recent approaches rely on deep learning and large amount of data specifically annotated for the task at hand [20, 7, 13], but, as for many other computer vision problems, getting such annotations is a cumbersome process. A popular solution is crowdsourcing that can spread the efforts for annotating data significantly [7]. Nonetheless, it introduces additional expenses and the resulting annotations produced by non-experts may not be satisfying.

An alternative approach is to reduce the amount of required manual annotations for learning. One way of doing this is through data augmentation which can be achieved by performing appropriate image transformations [29]. A dif-



(a) Training: We exploit some manual labels, as for Image I_1 , in a standard supervised fashion, and geometric constraints, as between Images I_2 and I_3 : The labels predicted for Image I_2 should be consistent with the labels predicted for Image I_3 .



(b) Testing: Segmentation from a single color image. Because we can exploit many training sequences without any labels, we can outperform supervised learning.

Figure 1: Our approach exploits some manual labels and geometric consistency on image sequences to train a network to perform semantic segmentation. At test time, the network predicts a dense segmentation from a single color image.

ferent option is to use synthetic data [28, 1]. However, creating synthetic data requires the cumbersome task of building realistic 3D models. Such approaches hence introduce additional difficulties as the domain gap between synthetic and real data needs to be bridged.

In this paper, we show how semantic segmentation learning can be cast into a semi-supervised framework. A standard technique from 'general' semi-supervised learning is to add constraints on pairs of unlabeled training samples that are close to each other, enforcing the fact that such two samples should belong to the same category. In the case of semantic segmentation learning, we can introduce similar semi-supervised constraints, enforcing the fact that image locations that correspond to the same 3D point should have the same label. As we show in Figure 1, together with standard supervised terms from the labeled images, these constraints result in a powerful learning process exploiting the 3D geometry nature of the problem. In fact, starting from RGB-D sequences with a few annotated frames, our results show that we can keep incorporating RGB-D sequences without any manual labels to improve the overall performance. This makes our approach very convenient since such sequences only need to be captured, without the effort of manually annotating them.

To demonstrate this idea, we make use of RGB-D image sequences of rigid scenes, and a very small number of manually annotated frames. We use such sequences because they provide the geometric information required to introduce our semi-supervised constraints, while being easily acquired with suitable cameras, and automatically registered using robust geometric algorithms. Alternatively, automated dense SLAM systems could be used to acquire such information for rigid scenes with a color camera [11, 36, 5], or for deformable scenes with an RGB-D camera [24, 34].

In short, our goal is not to develop a new semantic segmentation method or to improve performance on existing benchmarks, but to show that when multiple views of the same scene are available, enforcing geometric constraints with semi-supervised learning is a powerful framework for learning semantic segmentation when only a small fraction of the available data is annotated.

We demonstrate our semi-supervised training pipeline on different segmentation problems. We considered the ScanNet [7] and LabelFusion [22] datasets because they provide the input data suitable to our approach. First, we apply our method to a 4-class segmentation problem derived from the ScanNet dataset. For the experiments, we compare our method to a supervised approach. While supervised approach is trained using all of the available annotations, we show that our approach can achieve comparable results even after reducing the amount of manual annotations for training to a small fraction. Second, we apply our method to segmenting objects in a cluttered scene where many par-

tial occlusions are present and annotations typically include only parts of the objects. We show that with our method, only one manually labeled image is sufficient for segmenting a complete scene.

2. Related Work

In this section, we briefly discuss related work on the aspects of semantic segmentation, general semi-supervised learning, and also recent methods for learning depth prediction from single images, as they also exploit geometric constraints similar to our approach.

2.1. Supervised Semantic Segmentation with Deep Networks

Supervised semantic segmentation algorithms rely on principles that for a given image, the algorithm learns to output segmentation prediction that is similar to its ground truth annotation. In contrast to classification tasks, where a single label is required per image, semantic labels are on pixel-wise level. Prior to deep learning, Conditional Random Fields [27, 26] were a popular method for tackling this task.

Introduction of deep learning has made a large impact on the task of semantic segmentation. Fully Convolutional Networks (FCN) [20] allowed segmentation prediction for input of arbitrary size. In this setting, standard classification task networks [31, 14] are utilized and fully connected layers transformed into convolutions. FCNs use deconvolutional layers that learn the interpolation for upsampling process. Other works including SegNet [4], U-Net [29], and DeepLab [6] rely on similar architectures. Such works have been applied to a variety of segmentational tasks [29, 2, 23].

In our experiments, we use the U-Net architecture, because it is simple yet very powerful. However, any other architecture could be used instead.

2.2. Semi-Supervised Learning with Deep Networks

The main limitation of supervised methods is the availability of ground truth labels. In contrast, semi-supervised learning is a general approach aiming at exploiting both labeled and unlabeled training data. Some approaches rely on adversarial networks to measure the performance of unlabeled data [9, 10, 18, 15]. More in line with our work are the popular consistency-based models [19, 32, 3]. These methods enforce the model output to be consistent under small input perturbations. As explained in [3], consistency-based models can be viewed as a student-teacher model: To measure the consistency of a model f , or the student, its predictions are compared to the predictions of a teacher model g , a different trained model, while at the same time applying small input perturbations.

The Π -model [19] is a recent method using a consistency-based model where the student is its own

teacher, *i.e.* $f = g$. It relies on a cross-entropy loss term applied to labeled data only and an additional term that penalizes differences in predictions for small perturbations of input data. Our semi-supervised approach is closely related to the Π -*model* but relies on geometric consistency instead of the input perturbations.

2.3. Single-View Depth Estimation

Because of view warping, our approach is also related to recent work on unsupervised single-view depth estimation. Both Zhou *et al.* [36] and Godard *et al.* [11] proposed an unsupervised approach for learning depth estimation from video data. This is done by learning to predict a depth map so that a view can be warped into another one. This research direction became quickly popular, and has been extended since by many authors [35, 21, 33, 12].

Our work is related to these methods as it also introduces constraints between multiple views, by using warping. However, since we focus on semantics and not geometry, an input from the user is still required to indicate the different categories.

3. Method

We assume we are given a small set of registered images and their corresponding depths captured in one or several scenes and annotated by a user:

$$\mathcal{S} = \{e_i = (I_i, A_i, D_i, T_i, q_i)\}_i,$$

where I_i is a color image, A_i is its manual annotations, D_i is its depth map, T_i is the corresponding camera pose, and q_i is the index of the sequence. We are also given a set of similar examples, but for which there is no available manual annotations:

$$\mathcal{U} = \{e_j = (I_j, D_j, T_j, q_j)\}_j.$$

The samples in \mathcal{U} can be from the same sequences as the samples in \mathcal{S} but we can also have samples in \mathcal{U} from sequences that do not appear in \mathcal{S} . In other words, we can have scenes for which no manual labels are available and only geometric consistency can be exploited.

We would like to train a network $f(\cdot)$ using these data to segment views from novel scenes using only a color image as input.

3.1. Automatic Warping of the Manual Annotations

As shown in Fig. 2, by warping the manual annotations from \mathcal{S} to the images in \mathcal{U} from the same sequences, we can obtain easily additional annotations for these images. In other terms, we can generate annotations A_i for some of the images in \mathcal{U} , provided they are from the same sequence as a sample in \mathcal{S} and overlap its point of view.

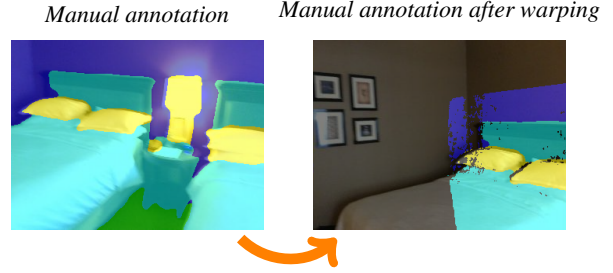


Figure 2: By warping the manual annotations to the non-labeled images, we can easily obtain additional annotations. We consider these additional annotations like the manual annotations and use them in the supervised loss term. Nevertheless, the semi-supervised geometric consistency term still has a significant benefit.

We consider these additional annotations like the manual annotations, even if they are obtained automatically, and we will use them in a supervised way. However, these annotations are only partial: Parts of images in \mathcal{U} will remain unlabeled if they are not seen in images in \mathcal{S} , and some images in \mathcal{U} will remain completely unlabeled if they do not belong to a sequence present in \mathcal{S} . These unlabeled parts can then be exploited by our semi-supervised terms.

In practice, due to errors in depth maps, registration, or manual annotation mistakes, the manual annotations A_i may be in conflict with each other when warped to the same image: For a pixel of an image in \mathcal{U} , we may have several possible classes. If it is the case, we keep the most frequent class. If there are still several possible classes, we select one randomly, however this case is extremely rare in practice.

3.2. Semi-Supervised Learning for Semantic Segmentation

To train f , we propose to minimize the following loss function for our semi-supervised approach over its parameters Θ :

$$L = L_S + \lambda L_G, \quad (1)$$

where L_S is a loss term for supervised learning, L_G is a loss term introducing our geometric consistency constraints, and λ is a regularization factor. For L_S , we use a standard term for supervised semantic segmentation:

$$L_S = \sum_{e \in \mathcal{S} \cup \mathcal{U}} l_{CE}(f(I(e); \Theta), A(e)), \quad (2)$$

with l_{CE} the cross-entropy function comparing the network prediction $f(I; \Theta)$ for image I and the manual annotation A . $I(e)$ and $A(e)$ simply denote the image and annotation for sample e . As explained in Section 3.1, for the samples in \mathcal{U} we use the annotations obtained automatically. There are samples in \mathcal{U} with no annotations and we simply ignore them.

To exploit unlabeled images and geometric consistency, we introduce the L_G loss term, which penalizes the differences in predicted probabilities:

$$L_G = \sum_{e \in \mathcal{U}} \sum_{e' \in \mathcal{N}(e)} |f(I(e); \Theta) - \text{Warp}_{e' \rightarrow e}(f(I(e'); \Theta))|, \quad (3)$$

where $\mathcal{N}(e)$ is a set of samples with a point of view that overlaps with the point of view of e . In practice, we simply use the frames from the same sequence as e . $\text{Warp}_{e' \rightarrow e}(P')$ warps labels P' for sample e' to the view for sample e . More details about the Warp function are given below. We consider prediction $f(I(e'); \Theta)$ as a teacher prediction and, similarly to the Π -model [19], it is treated as a constant when calculating the update of the network parameters. We use the ℓ_1 norm to compare the predicted probabilities.

3.3. Label Warping

To implement the warp function $P = \text{Warp}_{e' \rightarrow e}(P')$, we rely on the method used in [36] for intensity image warping. P' is a set of probability maps, one for each possible label, for a source sample e' . The warp function provides a probability map P for the labels of the target sample e , obtained by warping P' using the depth map for e' and the rigid motion between e' and e . Given the 2D location p in homogeneous coordinates and the depth d of a pixel for the target sample, we can compute the 2D location p' of the corresponding 2D point in the source sample e' :

$$p' = K T_{e \rightarrow e'} d K^{-1} p, \quad (4)$$

where K is the matrix of camera internal parameters, $T_{e \rightarrow e'}$ is the rigid motion from the target sample to the source sample. Since p usually lies between integer pixel locations, we use the differentiable bilinear interpolation from [16] to compute the final probabilities for $P'(p')$ from the 4 neighbouring pixels.

The advantage of this transformation is that it is differentiable, and can thus be used in the loss function of Eq. (1) to train the network.

In practice, not every pixel in the target sample has a correspondent in the source sample, and we ignore them in the loss function. This can happen because depth is not necessarily available for every pixel when using depth cameras, and because some pixels in the target sample may not be visible in the source sample, because they are occluded or, simply, because they are not in the field of view of the source sample. We detect if a pixel is occluded by comparing the original source depth at the mapped location to the transformed target depth given by the third coordinate of p' . If the difference between the depths is large, this means that the pixel is occluded and does not correspond to the same physical 3D point.

3.4. Network Initialization

To initialize the network $f(\cdot; \Theta)$, we first train it only based on the L_S loss term. This avoids the problem of converging to a bad local minimum introduced by the term L_G . As it is the case with other consistency-based models, minimizing L_G may fall in a solution where a single class is predicted for all the image locations. Even though tuning hyper-parameter λ more carefully might resolve this problem, we noticed that using this pre-training step makes the convergence to a correct model easier.

3.5. Network Architecture

We implement the network f as a U-Net architecture [29], with 5 layers for both the encoding and decoding parts. For the encoder, the number of features in the first layer is 32 and doubles up for every additional layer, and the decoder is symmetric to the encoder. We use convolutional filters of size 3 and apply reflection padding. Max-pooling layers use regions of size 2. All layers use ReLU activations except for the output layer, which uses the Softmax activation to predict segmentation probabilities. Other architectures could be used but U-Net proved to be both convenient and powerful enough for our purpose.

4. Evaluation

We evaluate our approach we call S4-Net on two different segmentation problems. We use the ScanNet dataset [7] and evaluate our approach on a 4-class segmentation problem demonstrating the influence of the number of annotated images on the final performance. Additionally, we evaluate the performance of S4-Net on the task of segmenting objects on the LabelFusion dataset [22].

Training Details: For all experiments, we set the λ factor in the loss function to 0.1. For different loss terms we use different batch sizes. The batch size for L_S is set to 4. Since L_G predicts larger number of segmentations for each iteration, we set the corresponding batch size to 1. We use the Adam optimizer [17] with initial learning rate of 10^{-4} and train the network until convergence. The input images are resized to 320×242 . As mentioned in Section 3.4, for better convergence, we pre-train the network only using the L_S term.

4.1. Segmenting 4 Classes on ScanNet

For our first experiment, we evaluate our method on *structural classes*, as defined in the NYU-Depth dataset [30]. Objects are classified to reflect their physical role in the scene: *ground*, *permanent structures* (structures that do not move such as walls and ceilings), *furniture* and *props* (easily movable objects).

Unfortunately, the NYU-Depth dataset is small and the camera poses are not provided. We therefore turned to the

ScanNet dataset [7]. It is organized into different scenes and for each scene, and BundleFusion [8] was used to register the RGB-D images. Furthermore, the dataset provides annotated 3D reconstructions of individual scenes and respectively the annotation mappings for each of the individual frames. Since the ScanNet dataset provides annotation mappings to NYU-Depth segmentation classes, we did not have to create any manual annotations ourselves.

As this dataset was annotated by a crowd sourcing community, the same types of objects can be annotated with different classes across the different scenes, or might not be annotated at all in some cases. Mapping to a 4-class semantic segmentation problem helps to alleviate this issue, but does not solve it completely.

In this experiment, we evaluate the behavior of S4-Net as we vary the number of manual annotations that are used for training. For each scene in the training set, we therefore discard uniformly desired number of annotations and apply our approach. We compare S4-Net to the supervised learning approach with and without annotation warping in Figure 3. More precisely, we use the following sets:

- The training set consists of the first 26 scenes from ScanNet.
- The test set consists of alternative scans of the scenes seen in the training set.
- The 'generalization test set' consists of scenes that were not in the training set. The performances on this set are the performances relevant for practical applications.

Additionally, during training, we use a validation set that includes alternative scans of the training scenes that are not in the test set nor in the generalization test set. It is used for validation of network parameters for different iterations during training. At the end of training, we keep the network with the highest validation accuracy for further evaluation.

The performances are measured with the accuracy of the network prediction compared to the provided ground truth annotations:

$$Acc = \frac{1}{\#images} \sum_{image} \frac{\#CorrectPredictions}{\#ValidAnnotations},$$

and the Intersection over Union (IOU) score.

Supervised learning with warped annotations significantly outperforms supervised learning without these annotations. Still, our S4-Net approach is able to improve the performances even further.

Finally, we show the ability of S4-Net to learn from additional scenes without any annotations. The annotated set \mathcal{S} consists of all manual annotations from the first 26 scenes. For the non-annotated set, we use scenes from the generalized test set *i.e.* scenes that appear neither in \mathcal{S} nor in the

test set. As shown in Table (c) of Figure 3, this significantly improves the performance. Figure 4 shows some qualitative results to give a visual idea of this improvement. The supervised approach with annotation warping often makes many small mistakes and enforcing geometric constraints during training of S4-Net managed to fix these mistakes.

4.2. Object Segmentation

For this experiment, we consider the LabelFusion dataset [22]. It contains RGB-D recordings of multi-object scenes and corresponding accurate poses, obtained through the ElasticFusion SLAM system [34]. LabelFusion provides accurate segmentations of the objects, which allows evaluating the segmentation results.

Given a sequence, we chose a single image that captures most of a scene, and used the annotation for this image for training. For this problem, we observed that standard cross-entropy for the supervised loss function performed poorly because most of the scene points belong to the background class, and we replaced it by the class-weighted cross-entropy [25]. This loss function down-weights the errors in prediction for frequently appearing classes and up-weights the errors for infrequently appearing classes. Hence, we only down-weight the errors for the background class to 0.1. This is the only change we make in respect to original definitions in method section.

For the experiment, we hence select a cluttered scene with different objects: an oil bottle, a tissue box, a blue funnel, a drill, a cracker box, a tomato soup can, and a spam can. Including the background class this defines an 8-class segmentation problem. Many partial occlusions happen in this scene, and as for the first experiment, simply warping the annotations is not sufficient. We show that S4-Net has the ability of improving on such regions.

Figure 5 shows some of the resulting segmentations. Supervised learning with annotation warping performs well. Even though the annotations can not be warped on every surface when two objects are close to each other, supervised learning is still able to learn segmentations for some of such regions because of the symmetry in the textures. However, perspective differences limit this generalization. The geometric constraint exploited by S4-Net improves the results on those regions by comparing such features warped under different perspectives. Finally, we performed a quantitative evaluation of the experiment. We calculate the IoU scores for both the supervised approach and S4-Net. Supervised approach with annotation warping achieves score of 86.7. S4-Net is able to reach even better results by achieving score of 88.4 and therefore outperforming the supervised approach.

	Accuracy						Intersection over Union					
	annotation percentage (%)						annotation percentage (%)					
	0.1	0.25	0.5	1	2	100	0.1	0.25	0.5	1	2	100
SL w/o annot. warping	64.2	68.3	73.6	81.3	88.3	98.6	37	40.2	43.4	51.4	60.4	92.9
SL w/ annot. warping	82.4	87.1	94.2	96.7	97.2	n/a	58	65.2	78.6	85.9	87.3	n/a
S4-Net	86.7	90.4	95.3	97	97.2	n/a	68.6	76.7	82.6	86.9	89	n/a

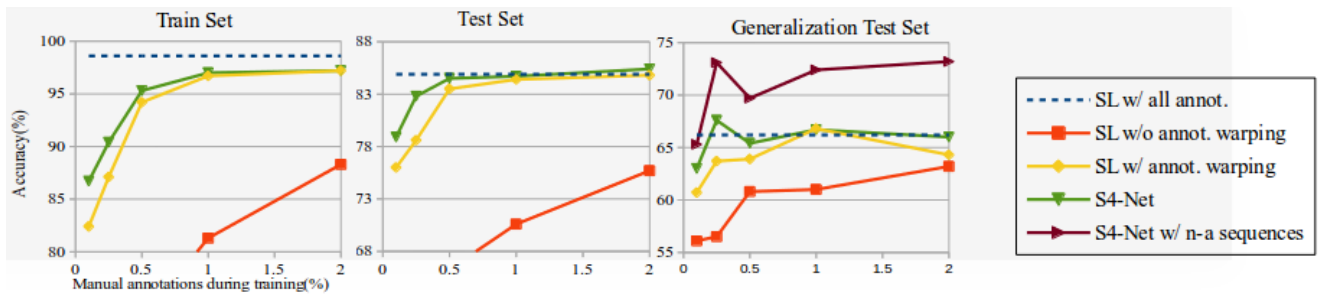
(a) Accuracy and Intersection-over-Union metrics on the training set.

	Accuracy						Intersection over Union					
	annotation percentage (%)						annotation percentage (%)					
	0.1	0.25	0.5	1	2	100	0.1	0.25	0.5	1	2	100
SL w/o annot. warping	60	63.1	66.3	70.6	75.7	84.9	33.2	35.7	37.1	41.6	46.1	60.8
SL w/ annot. warping	76	78.6	83.5	84.4	84.8	n/a	48.3	51.1	57.9	59.8	59.5	n/a
S4-Net	78.9	82.8	84.5	84.7	82	n/a	52.3	56.9	60.4	59.9	62.7	n/a

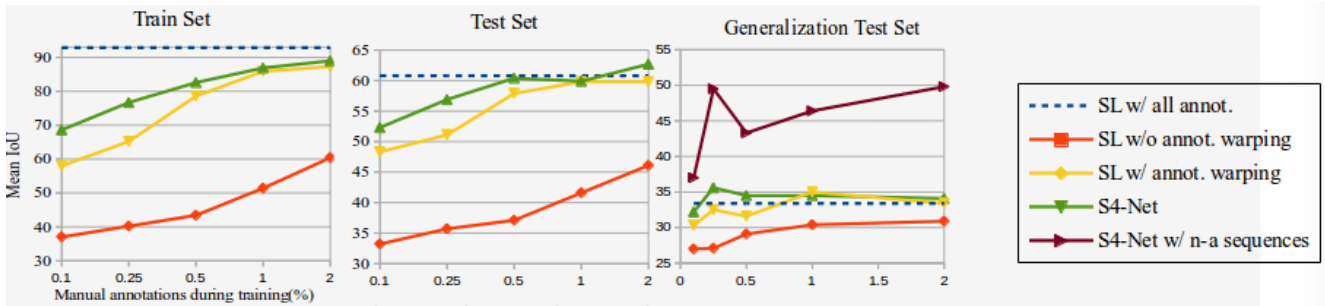
(b) Accuracy and Intersection-over-Union metrics on the test set.

	Accuracy						Intersection over Union					
	annotation percentage (%)						annotation percentage (%)					
	0.1	0.25	0.5	1	2	100	0.1	0.25	0.5	1	2	100
SL w/o annot. warping	56.1	56.5	60.8	61	63.2	66.2	27	27.1	29.1	30.4	30.9	33.4
SL w/ annot. warping	60.7	63.7	63.9	66.8	64.3	n/a	30.3	32.5	31.6	35	33.4	n/a
S4-Net	63	67.6	65.4	66.7	66	n/a	32.2	35.6	34.5	34.5	34.1	n/a
S4-Net w/ n-a sequences	65.3	73.1	69.7	72.4	73.2	n/a	37	49.5	43.3	46.4	49.8	n/a

(c) Accuracy and Intersection-over-Union metrics on the 'generalization test set'.



(d) Accuracy metric on different datasets for the different methods when varying the percentage of annotated images.



(e) Same for the Intersection-over-Union metric.

Figure 3: Datasets created from ScanNet, S4-Net average performances in respect to the percentage of annotations used during training. 'SL' stands for supervised learning, and 'S4-Net w/ n-a sequences' for S4-Net trained with additional non-annotated sequences. The performances on the 'generalisation test set' are the ones relevant for real applications.

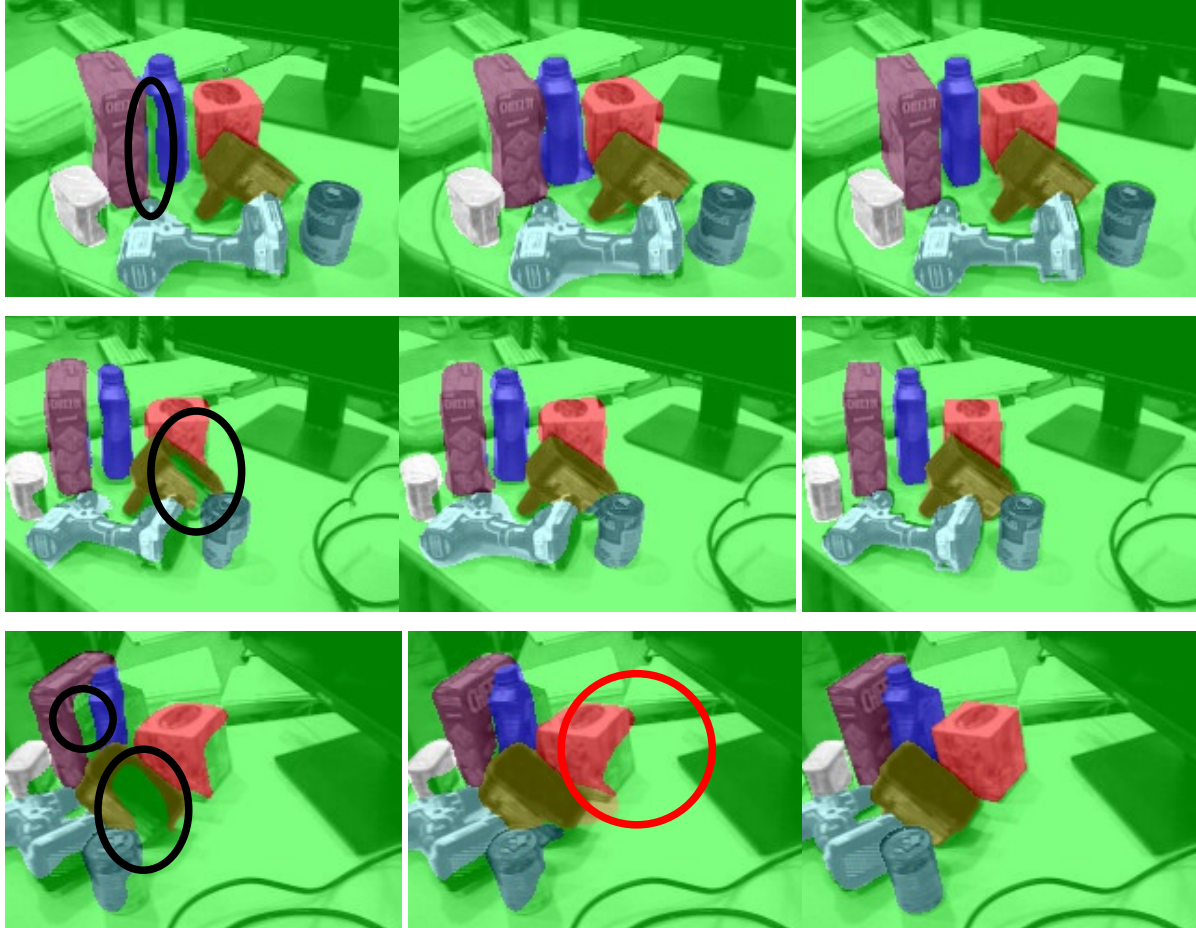


(a) Supervised approach

(b) S4-Net

(c) Ground Truth

Figure 4: Qualitative results on the generalization test set created from ScanNet. The supervised approach is able to predict correctly large parts of the segmentations on new scenes but still makes many mistakes. S4-Net can exploit additional non-labeled sequences of other scenes to correct most of these mistakes. The floor class is shown in **green**, the structure class in **blue**, the furniture class in **cyan**, and the props class in **yellow**.



(a) Supervised with annotation warping

(b) S4-Net

(c) Ground Truth Annotation

Figure 5: Qualitative results on the segmentation problem from FusionLabel. Annotation warping on its own is not enough to learn a whole scene from a single manual annotation. S4-NET improves performance on partially occluded objects up to some extent. Mistakes made by the supervised approach, shown with black ellipses, are corrected by S4-Net because of the influence of geometric constraint. However, S4-Net fails to deal with the regions shown with red ellipses that consistently output the wrong class.

5. Conclusion

We presented S4-Net, a semi-supervised semantic segmentation learning method with geometric constraints. We showed that semi-supervised learning with geometric constraints is a powerful framework to efficiently learn semantic segmentation when only a fraction of data is annotated. The current drawback of our implementation is that it requires depth data for the training images. As mentioned in the introduction, an option is to rely on automated dense SLAM systems to obtain such data from color images. Such systems are also in very fast development [11, 36, 5], and a very exciting possible extension of our work is to simultaneously learn to recover both geometry and semantic information from simple video sequences.

Acknowledgment

This work was supported by the Christian Doppler Laboratory for Semantic 3D Computer Vision, funded in part by Qualcomm Inc.

References

- [1] H. A. Alhaija, S. K. Mustikovela, L. M. Mescheder, A. Geiger, and C. Rother. Augmented Reality Meets Computer Vision: Efficient Data Generation for Urban Driving Scenes. *IJCV*, 2018. 2
- [2] A. Armagan, M. Hirzer, P. M. Roth, and V. Lepetit. Learning to Align Semantic Segmentation and 2.5D Maps for Geolocalization. In *CVPR*, 2017. 2

- [3] B. Athiwaratkun, M. Finzi, P. Izmailov, and A. G. Wilson. Improving Consistency-Based Semi-Supervised Learning with Weight Averaging. *arXiv preprint arXiv:1806.05594*, 2018. 2
- [4] V. Badrinarayanan, A. Kendall, and R. Cipolla. SegNet: A Deep Convolutional Encoder-Decoder Architecture for Image Segmentation. *TPAMI*, 2017. 2
- [5] M. Bloesch, J. Czarnowski, R. Clark, S. Leutenegger, and A. J. Davison. CodeSLAM - Learning a Compact, Optimisable Representation for Dense Visual SLAM. In *CVPR*, 2018. 2, 8
- [6] L. Chen, G. Papandreou, I. Kokkinos, K. Murphy, and A. L. Yuille. DeepLab: Semantic Image Segmentation with Deep Convolutional Nets, Atrous Convolution, and Fully Connected CRFs. *TPAMI*, 2018. 2
- [7] A. Dai, A. X. Chang, M. Savva, M. Halber, T. Funkhouser, and M. Niessner. ScanNet: Richly-Annotated 3D Reconstructions of Indoor Scenes. In *CVPR*, 2017. 1, 2, 4, 5
- [8] A. Dai, M. Nießner, M. Zollöfer, S. Izadi, and C. Theobalt. BundleFusion: Real-time Globally Consistent 3D Reconstruction using On-the-fly Surface Re-integration. *TOG*, 2017. 5
- [9] Z. Dai, Z. Yang, F. Yang, W. W. Cohen, and R. Salakhutdinov. Good Semi-supervised Learning That Requires a Bad GAN. In *NIPS*, 2017. 2
- [10] C. N. dos Santos, K. Wadhawan, and B. Zhou. Learning Loss Functions for Semi-supervised Learning via Discriminative Adversarial Networks. *arXiv preprint arXiv:1707.02198*, 2017. 2
- [11] C. Godard, O. Mac Aodha, and G. J. Brostow. Unsupervised Monocular Depth Estimation with Left-Right Consistency. In *CVPR*, 2017. 2, 3, 8
- [12] C. Godard, O. Mac Aodha, and G. J. Brostow. Digging Into Self-Supervised Monocular Depth Estimation. *arXiv preprint arXiv:1806.01260*, 2018. 3
- [13] K. He, G. Gkioxari, P. Dollár, and R. B. Girshick. Mask R-CNN. In *ICCV*, 2017. 1
- [14] K. He, X. Zhang, S. Ren, and J. Sun. Deep Residual Learning for Image Recognition. In *CVPR*, 2016. 2
- [15] W.-C. Hung, Y.-H. Tsai, Y.-T. Liou, Y.-Y. Lin, and M.-H. Yang. Adversarial Learning for Semi-supervised Semantic Segmentation. In *BMVC*, 2018. 2
- [16] M. Jaderberg, K. Simonyan, A. Zisserman, and K. Kavukcuoglu. Spatial Transformer Networks. In *NIPS*, 2015. 4
- [17] D. P. Kingma and J. Ba. Adam: A Method for Stochastic Optimization. In *ICLR*, 2015. 4
- [18] A. Kumar, P. Sattigeri, and P. T. Fletcher. Improved Semi-supervised Learning with GANs using Manifold Invariances. In *NIPS*, 2017. 2
- [19] S. Laine and T. Aila. Temporal Ensembling for Semi-Supervised Learning. In *ICLR*, 2017. 2, 4
- [20] J. Long, E. Shelhamer, and T. Darrell. Fully Convolutional Networks for Semantic Segmentation. In *CVPR*, 2015. 1, 2
- [21] R. Mahjourian, M. Wicke, and A. Angelova. Unsupervised Learning of Depth and Ego-Motion from Monocular Video Using 3D Geometric Constraints. In *CVPR*, 2018. 3
- [22] P. Marion, P. R. Florence, L. Manuelli, and R. Tedrake. LabelFusion: A Pipeline for Generating Ground Truth Labels for Real RGBD Data of Cluttered Scenes. In *ICRA*, 2018. 2, 4, 5
- [23] A. Milioto, P. Lottes, and C. Stachniss. Real-Time Semantic Segmentation of Crop and Weed for Precision Agriculture Robots Leveraging Background Knowledge in CNNs. In *ICRA*, 2018. 2
- [24] R. A. Newcombe, D. Fox, and S. M. Seitz. Dynamicfusion: Reconstruction and Tracking of Non-Rigid Scenes in Real-Time. In *CVPR*, 2015. 2
- [25] S. Panchapagesan, M. Sun, A. Khare, S. Matsoukas, A. Mandal, B. Hoffmeister, and S. Vitaladevuni. Multi-Task Learning and Weighted Cross-Entropy for DNN-Based Keyword Spotting. In *INTERSPEECH*, 2016. 5
- [26] N. Plath, M. Toussaint, and S. Nakajima. Multi-class image segmentation using conditional random fields and global classification. In *ICML*, 2009. 2
- [27] J. Reynolds and K. P. Murphy. Figure-ground segmentation using a hierarchical conditional random field. In *CRV*, 2007. 2
- [28] S. R. Richter, V. Vineet, S. Roth, and V. Koltun. Playing for Data: Ground Truth from Computer Games. In *ECCV*, 2016. 2
- [29] O. Ronneberger, P. Fischer, and T. Brox. U-Net: Convolutional Networks for Biomedical Image Segmentation. In *MICCAI*, 2015. 1, 2, 4
- [30] N. Silberman, D. Hoiem, P. Kohli, and R. Fergus. Indoor Segmentation and Support Inference from RGBD Images. In *ECCV*, 2012. 4
- [31] K. Simonyan and A. Zisserman. Very Deep Convolutional Networks for Large-Scale Image Recognition. *ICLR*, 2015. 2
- [32] A. Tarvainen and H. Valpola. Mean teachers are better role models: Weight-averaged consistency targets improve semi-supervised deep learning results. In *NIPS*, 2017. 2
- [33] C. Wang, J. M. Buenaposada, R. Zhu, and S. Lucey. Learning Depth from Monocular Videos using Direct Methods. In *CVPR*, 2018. 3
- [34] T. Whelan, R. F. Salas-Moreno, B. Glocker, A. J. Davison, and S. Leutenegger. ElasticFusion: Real-time dense SLAM and light source estimation. *I. J. Robotics Res.*, 2016. 2, 5
- [35] Z. Yin and J. Shi. GeoNet: Unsupervised Learning of Dense Depth, Optical Flow and Camera Pose. In *CVPR*, 2018. 3
- [36] T. Zhou, M. Brown, N. Snavely, and D. G. Lowe. Unsupervised Learning of Depth and Ego-Motion from Video. In *CVPR*, 2017. 2, 3, 4, 8